Observation of hybrid state of Tamm and surface plasmon-polaritons in one-dimensional photonic crystals

Cite as: Appl. Phys. Lett. **103**, 061112 (2013); https://doi.org/10.1063/1.4817999
Submitted: 09 July 2013 • Accepted: 25 July 2013 • Published Online: 07 August 2013

B. I. Afinogenov, V. O. Bessonov, A. A. Nikulin, et al.

Observation of hybrid state of Tamm and surface plasmon-polaritons in one-dimensional photonic crystals

B. I. Afinogenov, V. O. Bessonov,[a] A. A. Nikulin, and A. A. Fedyanin[b]
Faculty of Physics, Lomonosov Moscow State University, Moscow 119991, Russia

(Received 9 July 2013; accepted 25 July 2013; published online 7 August 2013)

Experimental observation of hybrid mode of Tamm plasmon-polariton and surface plasmon-polariton is reported. The hybrid state is excited in one-dimensional photonic crystal terminated by semitransparent metal film under conditions of total internal reflection for transverse-magnetic-polarized light. Coupling between Tamm and surface plasmon-polaritons leads to repulsion of their dispersion curves controlled by metal film thickness. © *2013 AIP Publishing LLC*.
[http://dx.doi.org/10.1063/1.4817999]

Surface electromagnetic waves (SEWs) excited in photonic crystals (PCs) have been intensively studied last years.[1–4] These states are analogues of surface plasmon-polaritons (SPPs) propagating at the interface between metal and dielectric. Excitation of SEW and SPP requires fulfilment of phase-matching conditions for the tangential component of the wave vector, which can be satisfied, for example, under total internal reflection in the Kretschmann scheme.

Tamm plasmon-polariton (TPP) is another surface mode which can be excited at the photonic crystal surface. It is an optical analogue of Tamm state,[5] which is electronic density localization at the boundary of periodic atomic potential, and appears as electromagnetic field localization at the boundary of photonic crystal and metal.[6,7] Contrary to SEW and SPP, Tamm plasmon-polaritons do not require phase-matching conditions for the tangential component of wave vector and can be excited at any angle of incidence. However, boundary conditions for the normal wave vector component are critical for TPP. Experimentally, TPPs manifest themselves as narrow absorption resonances in reflectance spectra of metal/PC systems.[6] TPPs exist for both transverse electric (TE) and transverse magnetic (TM) polarizations, while their spectral positions depend on the thickness of the PC topmost layer bounding to the metal. The uprise of the TPP in magnetophotonic crystals leads to enhancement of magneto-optical effects such as Faraday rotation.[8] TPPs coupled with other excitations such as excitons or microcavity modes have been explored last years[9–12] due to prospectives of the TPP application in new compact lasers.[13–16] Such optical states called as "hybrid" ones can be detected as a series of non-overlapping resonances in reflectance spectra. In a photonic crystal terminated by semitransparent metal film under total internal reflection SPP and TPP can be excited simultaneously[17] as it is schematically shown in Fig. 1. Coupling between SPP localized at the metal surface and TPP localized at the metal/PC interface might lead to appearance of the TPP-SPP hybrid state.

In this paper, experimental observation of the TPP-SPP hybrid mode excited in the Au/PC structure in the Kretschmann configuration is reported. It is shown that Tamm and plasmon components of the hybrid mode are revealed as two repulsing resonances. Dispersion curve of plasmonic component of the hybrid state is shifted to the longer wavelengths relative to the initial SPP dispersion curve. The dependence of the repulsion of Tamm and plasmon components of hybrid state on the metal film thickness is studied numerically.

The studied samples of distributed Bragg reflectors consisted of 6 pairs of ZrO_2/SiO_2 quarter-wavelength-thick layers deposited on quartz substrate using thermal evaporation. The layer thicknesses obtained from the scanning electron microscopy image of the sample cleavage were 110 nm (ZrO_2) and 145 nm (SiO_2), which correspond to the Bragg wavelength of $\lambda_B = 850$ nm. According to the calculations, Tamm plasmon-polariton is efficiently excited if the PC topmost layer has either higher refractive index (ZrO_2) and quarter-wavelength optical thickness, or lower refractive index (SiO_2) and optical thickness larger than $\lambda_B/4$. Optimal thickness of the topmost (SiO_2) layer was numerically estimated as 225 nm, therefore additional 80-nm-thick layer of SiO_2 was deposited on a PC surface. The resultant structure was covered by a semitransparent 30-nm-thick gold film

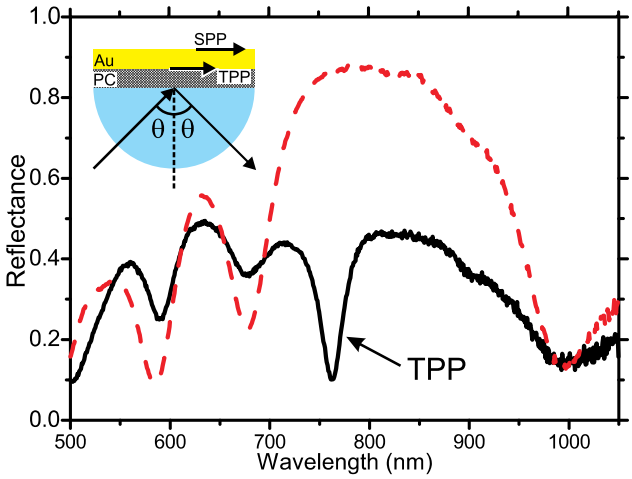

FIG. 1. Experimental reflectance spectra of photonic crystal (dashed curve) and Au/PC (solid curve) samples at $\theta = 30°$ for TM polarization. Inset: schematic of the experiment.

[a]Also at A. N. Frumkin Institute of Physical Chemistry and Electrochemistry, Russian Academy of Science, Moscow 119071, Russia
[b]Electronic mail: fedyanin@nanolab.phys.msu.ru

allowing both good field localization in the TPP mode and the SPP excitation. The relatively low number of periods (six) of PC provides sufficient penetration of the electromagnetic field through the PC under conditions of a total internal reflection for the SPP and TPP appearances. Bare photonic crystal of the same parameters and a 30-nm-thick gold film on fused quartz substrate were reference samples.

Reflection spectra were measured with the 1-nm resolution using polarized collimated beam. Angular dependences were measured by the θ–2θ goniometer provided 0.005° accuracy. Sample was set by immersion oil on a cylindrical prism ($n_{prism} = 1.52$) for covering wide range of angles of incidence θ (inset in Fig. 1). Numerical simulations were performed using transfer matrix technique with realistic dielectric function dispersion for gold from Ref. 18 and assuming refractive indexes of SiO_2 and ZrO_2 as 1.46 and 1.95, respectively.

Fig. 1 shows reflection spectra $R(\lambda)$ of the photonic crystal and the Au/PC sample measured at $\theta = 30°$. Photonic band-gap (PBG) is seen for PC between 700 nm and 950 nm. Transmittance inside the PBG is relatively high being approximately equal to 0.1 indicating notable light transit through photonic crystal. According to the calculations such transmittance value is optimal for efficient TPP excitation. Reflectivity spectrum of the Au/PC sample is flattened due to supplementary absorption in the gold layer. Maximal reflection in PBG is slightly below 0.5. A resonance appeared at 755 nm is spectrally located inside photonic band-gap and corresponds to the TPP excitation. Reflectance in the spectral region of the TPP is relatively low being less than 0.1 indicating a significant light tunnelling via TPP.

Fig. 2 shows $R(\lambda, \theta)$ for the TM polarization of incoming light, measured (Fig. 2(a)) and calculated (Fig. 2(b)). TPP dip inside photonic band-gap is observed for incident angles less than the angle of total internal reflection (41° for the used prism). Both TPP resonance and PBG become blue-shifted with the incident angle increase as perpendicular component of the wave vector decreases. For the incident angles exceeding the angle of total internal reflection the SPP phase matching conditions are satisfied. The SPP dip starts at $\theta = 42°$ and $\lambda = 1000$ nm and rapidly blue-shifts with increasing the angle of incidence. However, dispersion curve of the SPP component is considerably red-shifted comparing to that of SPP at the reference gold film. This is due to the SPP coupling with TPP which leads to repulsion of the resonances. Indeed, inset in Fig. 2(a) shows $R(\lambda, \theta)$ for the reference gold film. The dip corresponding to the SPP excitation appears at 42°. Spectral position of SPP measured at 50° for the reference sample is approximately 520 nm while for the Au/PC sample it is about 610 nm.

TPP and SPP cannot be excited independently at given angle of incidence or wavelength. They correspond to a common solution of the wave equation being a superposition of the electromagnetic wave localized at the metal/PC interface (TPP) and the mode localized at the metal/air interface (SPP) forming hybrid state. Fig. 2(b) shows calculated reflection spectra depending on the angle of incidence which is in a good agreement with experimental results. Slight discrepancy between experimental and modelled spectra appears due to angular divergence of the beam and focusing ability

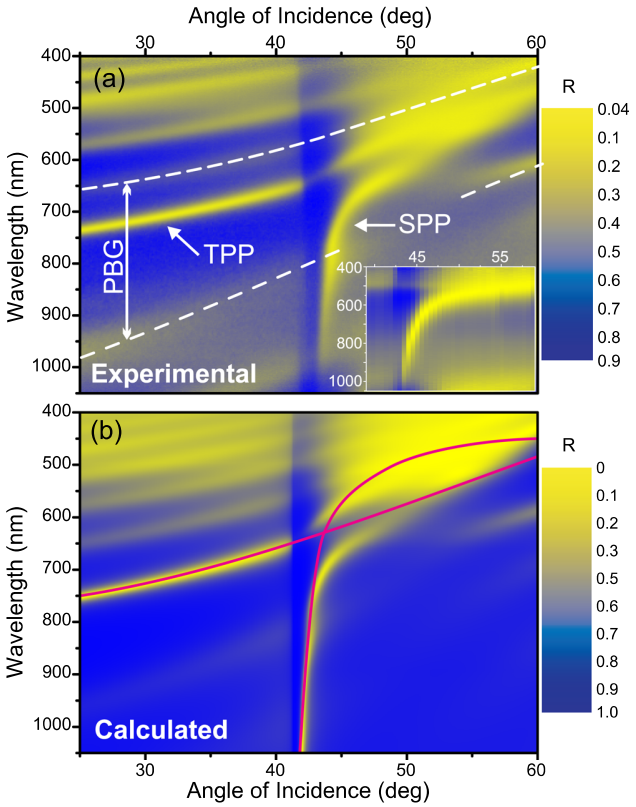

FIG. 2. (a) Image plot of the experimental reflectivity (R) spectrum of the Au/PC sample for TM polarization. Arrows indicate reflectivity dips visualizing dispersion curves of Tamm plasmon-polariton and surface plasmon-polariton. Dashed curves mark the photonic band-gap. Inset shows image plot of experimental reflectivity spectrum of a reference gold film for TM polarization. (b) Image plot of the calculated reflectivity spectrum for TM polarization. Solid curves are dispersion curves of TPP and SPP if they would be excited independently.

of cylindrical prism in the experiment. Comparison with dispersion curves calculated for uncoupled TPP and SPP shows clear repulsion of hybrid state components in the crossing point of reflectivity dips.

Fig. 3(a) shows $R(\lambda, \theta)$ measured for the TE polarized light when SPP propagation is forbidden and TPP is excited solely. Spectral position of the TPP resonances for TM and TE polarizations are different being at $\theta = 30°$ equal to 710 nm and 690 nm, respectively, due to polarization splitting. Spectral position of the TPP mode is located inside PBG and shifts to the shorter wavelengths approaching PBG edge with the increase of incidence angle. This is in agreement with numerical calculations shown in Fig. 3(b).

Numerical calculations were also performed to study how coupling of TPP and SPP depends on the thickness of the gold layer. Parameters of the model Au/PC structure were the same as in the experiment. Numerical results are shown in Fig. 4. For the 20-nm-thick gold film spectral repulsion between TPP and SPP resonances at $\theta = 43.5°$ is approximately 140 nm. With increasing thickness of the gold layer spectral splitting of TPP and SPP components of the hybrid state decreases since normalized overlap integral of exponential tails of SPP and TPP in the metal layer diminishes. For the films thicker than 60 nm TPP and SPP do not sense each other and repulsion of their dispersion curves becomes negligible.

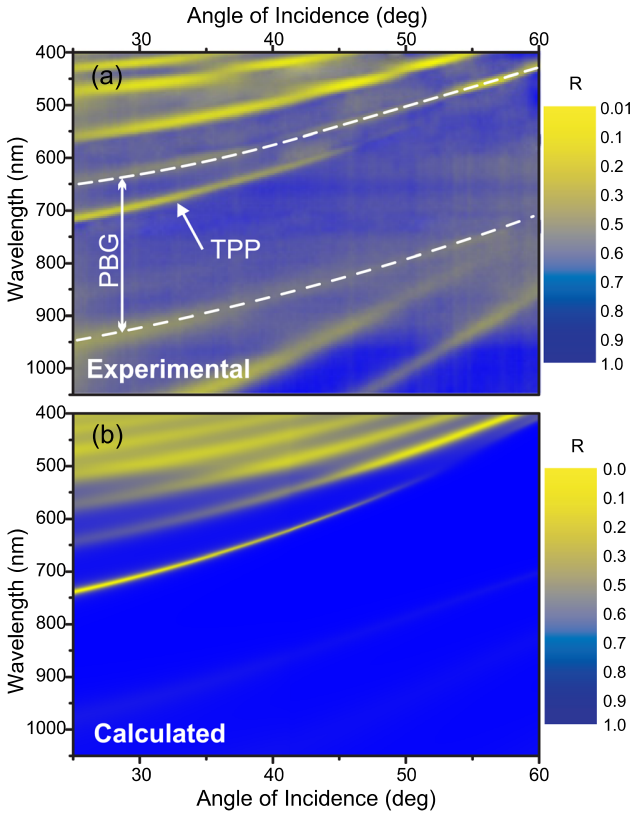

FIG. 3. (a) Image plot of the experimental reflectivity (R) spectrum of the Au/PC sample for the TE polarization. Arrow indicates dispersion curve of Tamm plasmon-polariton. Dashed curves mark the photonic band-gap. (b) Image plot of the calculated reflectivity spectrum for TE polarization.

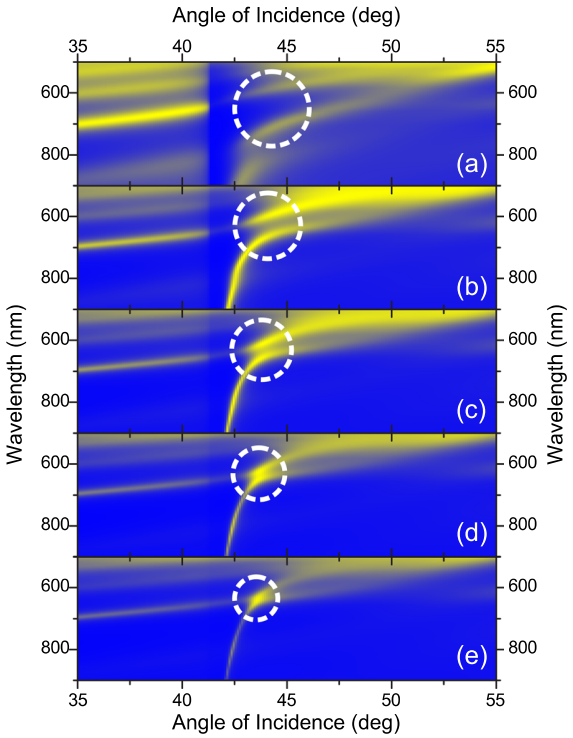

FIG. 4. Image plots of the reflectivity spectra for TM polarization calculated for thicknesses of gold layer of 20 nm (a), 40 nm (b), 50 nm (c), 60 nm (d), and 70 nm (e). Dashed circles emphasize the spectral-angular region of TPP and SPP dispersion curves repulsion in the hybrid state.

To proceed with interpretation of the observed effects we consider a model structure (Fig. 5(a)) formed by a metal slab of thickness d_M adjacent to a semi-infinite one-dimensional photonic crystal that is comprised of alternating dielectric layers of thicknesses d_1 and d_2. The dielectric constants of the metal slab and layers of the photonic crystal, ε_M, ε_1, and ε_2, respectively, are assumed to be real quantities: $\varepsilon_M < 0$ and $\varepsilon_{1,2} > 0$. The dielectric layer contacting with the metal has thickness $d_1 + \delta$. In the eigenmode with frequency ω the electric and magnetic fields, **E** and **H**, have the form

$$\mathbf{F}(\mathbf{R}, z, t) = \mathbf{F}(z)e^{i(\mathbf{KR}-\omega t)}, \quad (1)$$

where **F** stands for either **E** or **H**, **R** is the radius-vector in the surface xy-plane and **K** is the wavevector parallel to the xy-plane. In what follows the x-axis is chosen to be parallel to **K**. Then for the TM-mode the non-vanishing field components are H_y, $E_x = -i[\varepsilon(z)k]^{-1}dH_y/dz$, $E_z = -K[\varepsilon(z)k]^{-1}H_y$, whereas for the TE-mode they are E_y, $H_x = ik^{-1}dE_y/dz$, $H_z = Kk^{-1}H_y$ (where $k = \omega/c$ and the piecewise-constant function $\varepsilon(z)$ describes the spatial variation of the dielectric constant). It is convenient to introduce the notation

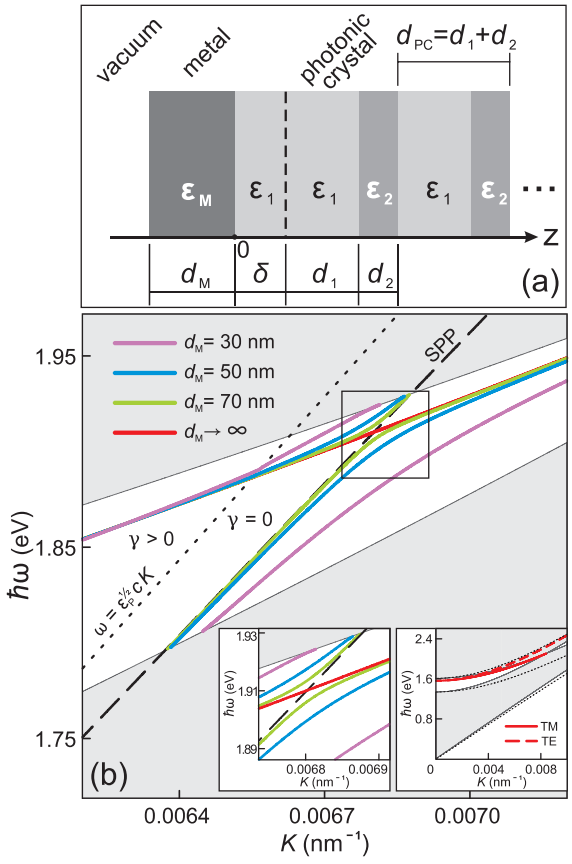

FIG. 5. (a) Model structure. (b) Dispersion of the TM TPP calculated for the model structure at specified values of d_M. Gray areas correspond to the bulk TM photonic bands of the infinite PC. Dashed line indicates the dispersion curve of the SPP at the vacuum/semi-infinite metal interface. Dotted line being the light line in the prism separates radiative ($\gamma > 0$) and non-radiative ($\gamma = 0$) regions. The area marked with the square is shown enlarged in the left inset. Right inset shows the dispersion curves of the TM and TE TPPs calculated for the semi-infinite metal/semi-infinite PC structure. Dotted lines represent the boundaries of the bulk TE photonic bands. The parameters used in calculations are the following: $\delta = 80$ nm, $d_1 = 146$ nm, $d_2 = 109$ nm, $\varepsilon_1 = \varepsilon_p = 2.13$, $\varepsilon_2 = 3.80$, $\varepsilon_M(\omega) = 1 - (\omega_p/\omega)^2$ with $\hbar\omega_p = 8.87$ eV.

$F_{\mathrm{TM}}(z) \equiv H_y(z)$, $F_{\mathrm{TE}}(z) \equiv E_y(z)$. The field in the Tamm eigenmode depends on z as follows ($\alpha = \mathrm{TM}, \mathrm{TE}$):

$$F_\alpha(z) = \begin{cases} A_\alpha e^{-iqz}, & z < -d_{\mathrm{M}} \\ B_\alpha e^{-\kappa_{\mathrm{M}} z} + C_\alpha e^{\kappa_{\mathrm{M}} z}, & -d_{\mathrm{M}} < z < 0, \\ D_\alpha u_\alpha(z) e^{iQ_\alpha z}, & z > 0 \end{cases} \quad (2)$$

where A_α, B_α, C_α, D_α are complex constants, $q = \sqrt{k^2 - K^2}$, $\kappa_{\mathrm{M}} = \sqrt{K^2 - \varepsilon_{\mathrm{M}} k^2}$. The quantity Q_α is the complex Bloch wave number corresponding to an evanescent Bloch wave inside the PBG. At $z > \delta$ the function $u_\alpha(z)$ is periodic with period $d_{\mathrm{PC}} = d_1 + d_2$. Explicit expressions for Q_α and $u_\alpha(z)$ are omitted for brevity sake and can be found elsewhere (see, e.g., Ref. 19).

Requirement of continuity of the tangential field components on the vacuum/metal and metal/photonic crystal interfaces leads to a set of four uniform linear equations with respect to four constants A_α, B_α, C_α, and D_α. Compatibility of these equations is attained by setting the determinant of the corresponding matrix equal to zero. This condition can be represented in the following form:

$$\frac{e^{-2i\Delta} - b_\alpha}{e^{-2i\Delta} + b_\alpha} = -\mu_\alpha \frac{\cosh L_{\mathrm{M}} + \nu_\alpha \sinh L_{\mathrm{M}}}{\nu_\alpha \cosh L_{\mathrm{M}} + \sinh L_{\mathrm{M}}}, \quad (3)$$

where

$$b_\alpha = \frac{(1 - r_\alpha^2) e^{i\Lambda_\alpha} + e^{iL_1}(r_\alpha^2 e^{-iL_2} - e^{iL_2})}{2 i r_\alpha e^{-iL_1} \sin L_2},$$

$$r_{\mathrm{TM}} = \frac{\varepsilon_1 q_2 - \varepsilon_2 q_1}{\varepsilon_1 q_2 + \varepsilon_2 q_1}, \quad r_{\mathrm{TE}} = \frac{q_2 - q_1}{q_1 + q_2},$$

and $\mu_{\mathrm{TM}} = i\varepsilon_1 \kappa_{\mathrm{M}} / (\varepsilon_{\mathrm{M}} q_1)$, $\mu_{\mathrm{TE}} = i\kappa_{\mathrm{M}} / q_1$, $\nu_{\mathrm{TM}} = i\kappa_{\mathrm{M}} / (\varepsilon_{\mathrm{M}} q)$, $\nu_{\mathrm{TE}} = i\kappa_{\mathrm{M}} / q$, $\Delta = q_1 \delta$, $L_{\mathrm{M}} = \kappa_{\mathrm{M}} d_{\mathrm{M}}$, $\Lambda_\alpha = Q_\alpha d_{\mathrm{PC}}$, $L_j = q_j d_j$, $q_j = \sqrt{\varepsilon_j k^2 - K^2}$, $j = 1, 2$. The roots of Eq. (3) determine the dispersion law of the Tamm polaritons: $\omega = \Omega_\alpha(K)$. Under condition $\omega < cK$ the wave in the vacuum becomes evanescent at $z < -d_{\mathrm{M}}$, which corresponds to the non-radiative Tamm mode (at arbitrary value of d_{M}). In this case Eq. (3) has roots at real values of both ω and K. At $\omega > cK$, the Tamm mode is radiatively decaying due to energy flow into the region $z < -d_{\mathrm{M}}$ where the Poynting vector has a non-zero z-component. As a result, at real K the eigenfrequencies of the Tamm modes are complex: $\omega = \Omega_\alpha(K) - i\gamma_\alpha(K)$, with $\gamma_\alpha(K) \to 0$ at $d_{\mathrm{M}} \to \infty$.

In experiment the prism providing the total internal reflection of the incident radiation is used and the longitudinal wavevector component is related to the angle of incidence θ as $\varepsilon_{\mathrm{P}}^{1/2} \omega \sin\theta / c$ (where ε_{P} is the dielectric constant of the prism). Consequently, one should deal with the dispersion dependence on the properly scaled argument: $\omega = \Omega_\alpha(\varepsilon_{\mathrm{P}}^{1/2} K)$. The numerical results are shown in Fig. 5(b). When the thickness of the metal slab is sufficiently small, excitation of the surface plasmon at the vacuum/metal interface noticeably modifies the dispersion of the Tamm polariton in the TM-mode.

In conclusion, we have obtained unambiguous experimental evidence of excitation of hybrid mode of Tamm and surface plasmon-polaritons in photonic crystal terminated by metal film. For TM polarized incoming light these two surface modes exist on opposite surfaces of the metal film. Tamm and plasmon components of hybrid state are revealed as two non-overlapping resonances. Their coupling leads to repulsion of dispersion curves, which can be controlled by the thickness of the metal layer. This phenomenon, together with the dependence of the resonance wavelength of the TPP on the thickness of the topmost layer of a PC, can be prospective for creating tunable plasmonic filters and sensors.

This work was supported by Russian Foundation for Basic Research (12-02-33107, 12-02-12092), Russian Ministry of Education and Science (14.513.11.0017), and Leading Russian Science Schools Grant (4375.2012.2).

[1]W. M. Robertson and M. S. May, Appl. Phys. Lett. **74**, 1800 (1999).
[2]I. V. Soboleva, E. Descrovi, C. Summonte, A. A. Fedyanin, and F. Giorgis, Appl. Phys. Lett. **94**, 231122 (2009).
[3]A. B. Khanikaev, A. V. Baryshev, M. Inoue, and Yu. S. Kivshar, Appl. Phys. Lett. **95**, 011101 (2009).
[4]I. V. Soboleva, V. V. Moskalenko, and A. A. Fedyanin, Phys. Rev. Lett. **108**, 123901 (2012).
[5]I. Tamm, Zeitschrift für Physik **76**, 849 (1932).
[6]M. Kaliteevski, I. Iorsh, S. Brand, R. A. Abram, J. M. Chamberlain, A. V. Kavokin, and I. A. Shelykh, Phys. Rev. B **76**, 165415 (2007).
[7]M. E. Sasin, R. P. Seisyan, M. A. Kaliteevski, S. Brand, R. A. Abram, J. M. Chamberlain, A. Yu. Egorov, A. P. Vasil'ev, V. S. Mikhrin, and A. V. Kavokin, Appl. Phys. Lett. **92**, 251112 (2008).
[8]T. Goto, A. V. Dorofeenko, A. M. Merzlikin, A. V. Baryshev, A. P. Vinogradov, M. Inoue, A. A. Lisyansky, and A. B. Granovsky, Phys. Rev. Lett. **101**, 113902 (2008).
[9]C. Symonds, A. Lemaître, E. Homeyer, J. C. Plenet, and J. Bellessa, Appl. Phys. Lett. **95**, 151114 (2009).
[10]R. Brückner, M. Sudzius, S. I. Hintschich, H. Fröb, V. G. Lyssenko, and K. Leo, Phys. Rev. B **83**, 033405 (2011).
[11]M. Kaliteevski, S. Brand, R. A. Abram, I. Iorsh, A. V. Kavokin, and I. A. Shelykh, Appl. Phys. Lett. **95**, 251108 (2009).
[12]H. Liu, X. Sun, F. Yao, Y. Pei, H. Yuan, and H. Zhao, Plasmonics **7**, 749 (2012).
[13]C. Symonds, G. Lheureux, J. P. Hugonin, J. J. Greffet, J. Laverdant, G. Brucoli, A. Lemaitre, P. Senellart, and J. Bellessa, Nano Lett. **13**, 3179 (2013).
[14]R. Brückner, A. A. Zakhidov, R. Scholz, M. Sudzius, S. I. Hintschich, H. Fröb, V. G. Lyssenko, and K. Leo, Nat. Photonics **6**, 322 (2012).
[15]C. Symonds, A. Lemaître, P. Senellart, M. H. Jomaa, S. Aberra Guebrou, E. Homeyer, G. Brucoli, and J. Bellessa, Appl. Phys. Lett. **100**, 121122 (2012).
[16]O. Gazzano, S. M. de Vasconcellos, K. Gauthron, C. Symonds, J. Bloch, P. Voisin, J. Bellessa, A. Lemaître, and P. Senellart, Phys. Rev. Lett. **107**, 247402 (2011).
[17]A. V. Baryshev, K. Kawasaki, P. B. Lim, and M. Inoue, Phys. Rev. B **85**, 205130 (2012).
[18]P. B. Johnson and R. W. Christy, Phys. Rev. B **6**, 4370 (1972).
[19]A. Yariv and P. Yeh, *Optical Waves in Crystals* (Wiley, New York, 1984), Vol. 5.